Meiotic crossover number and distribution are regulated by a dosage compensation protein that resembles a condensin subunit

Chun J. Tsai, David G. Mets, Michael R. Albrecht, Paola Nix, Annette Chan and Barbara J. Meyer

Genes & Dev. 2008 22: 194-211
Access the most recent version at doi:10.1101/gad.1618508

Meiotic crossover number and distribution are regulated by a dosage compensation protein that resembles a condensin subunit

Chun J. Tsai,[2] David G. Mets, Michael R. Albrecht,[3] Paola Nix,[1,4] Annette Chan,[1,5] and Barbara J. Meyer[6]

Howard Hughes Medical Institute, Department of Molecular and Cell Biology, University of California at Berkeley, Berkeley, California 97420, USA

Biological processes that function chromosome-wide are not well understood. Here, we show that the *Caenorhabditis elegans* protein DPY-28 controls two such processes, X-chromosome dosage compensation in somatic cells and meiotic crossover number and distribution in germ cells. DPY-28 resembles a subunit of condensin, a conserved complex required for chromosome compaction and segregation. In the soma, DPY-28 associates with the dosage compensation complex on hermaphrodite X chromosomes to repress transcript levels. In the germline, DPY-28 restricts crossovers. In many organisms, one crossover decreases the likelihood of another crossover nearby, an enigmatic process called crossover interference. In *C. elegans*, interference is complete: Only one crossover occurs per homolog pair. *dpy-28* mutations increase crossovers, disrupt crossover interference, and alter crossover distribution. Early recombination intermediates (RAD-51 foci) increase concomitantly, suggesting that DPY-28 acts to limit double-strand breaks (DSBs). Reinforcing this view, *dpy-28* mutations partially restore DSBs in mutants lacking HIM-17, a chromatin-associated protein required for DSB formation. Our work further links dosage compensation to condensin and establishes a new role for condensin components in regulating crossover number and distribution. We propose that both processes utilize a related mechanism involving changes in higher-order chromosome structure to achieve chromosome-wide effects.

[*Keywords*: X-chromosome dosage compensation; condensin; meiosis; crossover interference; epigenetics; DPY-28]

Supplemental material is available at http://www.genesdev.org.

Received September 24, 2007; revised version accepted November 15, 2007.

No biological processes that operate on the level of an entire metazoan chromosome are understood in detail. We show that two such processes, X-chromosome dosage compensation and meiotic crossover (CO) control, are linked through a shared protein. Dosage compensation is an essential regulatory process that equalizes expression of most X-linked genes between the sexes (XO or XY males and XX females), despite their twofold difference in X-chromosome dose. CO number and distribution are tightly controlled during meiosis to ensure proper chromosome segregation. The use of a common protein suggests that a related mechanism underlies these two seemingly disparate chromosome-wide processes.

In the nematode *Caenorhabditis elegans*, a dosage compensation complex (DCC) is targeted to both X chromosomes of hermaphrodites to reduce transcript levels by half, thereby achieving an X expression level in XX hermaphrodites similar to that in XO males (for review, see Meyer 2005). The DCC components DPY-27 and MIX-1 are members of the SMC (Structural Maintenance of Chromosomes) family of DNA-associated ATPases (Chuang et al. 1994; Lieb et al. 1998), and both resemble components of condensin, a highly conserved protein complex essential for the compaction, resolution, and segregation of mitotic and meiotic chromosomes from yeast to humans (Hagstrom et al. 2002; Yu and Koshland

[1]These authors contributed equally to this work.
Present addresses: [2]Department of Medicine and Department of Biochemistry, Stanford University Medical Center, Stanford, CA 94305, USA; [3]Finnegan, Henderson, Farabow, Garrett and Dunner, L.L.P., Palo Alto, CA 94304, USA; [4]Department of Biology, University of Utah, Salt Lake City, UT 84112, USA; [5]Cell and Molecular Imaging Center, Department of Biology, San Francisco State University, San Francisco, CA 94132 USA
[6]Corresponding author.
E-MAIL bjmeyer@berkeley.edu; FAX (510) 643-5584.
Article is online at http://www.genesdev.org/cgi/doi/10.1101/gad.1618508.

2003; Chan et al. 2004; for review, see Losada and Hirano 2005). Prototypical condensin includes not only a pair of SMC proteins, but also three non-SMC proteins of distinct CAP (Chromosome-Associated Polypeptide) families called CAP-D2, CAP-G, and CAP-H/Barren. The strong resemblance of DPY-27 and MIX-1 to condensin components suggests that the DCC might include homologs of all condensin subunits. The DCC component DPY-26 shares a small stretch of similarity with CAP-H, but other non-SMC subunits had not been found. The X localization of the condensin-like DCC suggests that dosage compensation in worms is mediated through changes in X-chromosome structure.

C. elegans dosage compensation recruited existing components used in more ancestral chromosome behaviors to the task of modulating gene expression. MIX-1, for example, functions not only in dosage compensation but also in chromosome segregation during mitosis and meiosis. MIX-1 partitions its roles in these two separate biological processes through its participation in two distinct complexes, the DCC and the mitotic–meiotic condensin II complex (Hagstrom et al. 2002; Chan et al. 2004). When MIX-1 associates with the DCC in hermaphrodites, it binds to X chromosomes (Lieb et al. 1998); when MIX-1 associates with condensin II in both sexes, it colocalizes with centromeres during mitosis (Hagstrom et al. 2002) and diplotene-diakinesis chromosomes during meiosis (Chan et al. 2004).

We show that DPY-28 is a bona fide homolog of CAP-D2 and a member of the DCC, thus strengthening the connection between the DCC and condensin. Moreover, DPY-28, like MIX-1, participates in two separate regulatory processes that preside over entire chromosomes. In addition to its sex-specific function in the transcriptional regulation of X-linked genes, DPY-28 plays an important and unexpected role in controlling CO distribution during meiosis.

Meiosis is a specialized cell cycle devoted to the production of haploid gametes. It is characterized by a single round of DNA replication followed by two rounds of cell division. During meiosis, chromosomes undergo striking morphological changes to facilitate several key events: pairing and synapsis of homologous chromosomes, reciprocal exchange of DNA between homologs (CO recombination), and chromosome segregation (for review, see Zickler and Kleckner 1999). Following meiotic DNA replication, the duplicated homologs align to achieve an intimate association via a highly ordered proteinaceous structure, the synaptonemal complex (SC). COs initiate prior to SC assembly but mature in the context of assembled SC. COs provide the physical connections between homologs required for proper orientation of chromosomes on the meiosis I spindle and thus for accurate segregation of homologs during the first meiotic division. Failure to form or properly place COs among meiotic chromosomes causes missegregation of homologs, resulting in aneuploidy and zygotic lethality, defects that underscore the importance of understanding the control of meiotic recombination.

The molecular mechanism of meiotic recombination is best characterized in budding yeast, and many of the recombination proteins are widely conserved among eukaryotes, including *C. elegans* (for review, see Villeneuve and Hillers 2001). Recombination events are initiated by formation of transient DNA double-strand breaks (DSBs) (Szostak et al. 1983; Sun et al. 1989) catalyzed by the type II topoisomerase-like protein Spo11p (Bergerat et al. 1997; Keeney et al. 1997). A DSB is resected to produce an intermediate with a 3′-overhanging ssDNA tail (Sun et al. 1991). Rad51p and Dmc1p, RecA-related strand-exchange proteins, bind to the ssDNA tails to form filamentous nucleoprotein structures that promote a search for homologous DNA (Ogawa et al. 1993; Sung 1994; Hong et al. 2001). When DNA homology is found, DNA strand invasion by one processed end produces a single-ended invasion product (Hunter and Kleckner 2001) that differentiates into either a CO or a non-CO (Allers and Lichten 2001; Hunter and Kleckner 2001).

Distribution of meiotic DSBs is nonuniform in many eukaryotic genomes (for review, see Petes 2001). Most DSBs occur in chromosomal regions that exhibit characteristics of open chromatin. Such regions include constitutively nucleosome-free areas (Kirkpatrick et al. 1999), transcription promoters that show nuclease-sensitivity (Ohta et al. 1994; Wu and Lichten 1994), and local areas of high GC base composition (Gerton et al. 2000). The number of local DSBs correlates with the recombination activity of a given chromosomal region; hence, most DSBs coincide with recombination hot spots. Although the molecular basis for hot-spot activity is not understood, it has been proposed that hot spots are located in accessible chromosomal regions that potentiate interactions between DNA and the recombination machinery.

Meiotic COs are also distributed nonrandomly along chromosomes; one CO discourages the occurrence of other COs nearby, such that two COs rarely occur close together. This phenomenon, called crossover interference, is widely observed across phyla (Zickler and Kleckner 1999). Crossover interference allows a more even distribution of chiasmata among chromosomes that vary in size so even the smallest chromosome has at least one chiasma, a necessity for proper segregation of chromosomes. Recent evidence from budding yeast showed that interference begins prior to the onset of stable strand exchange and is independent of SC (Borner et al. 2004; Fung et al. 2004). Although the mechanism underlying interference has not been defined, models have been proposed (Borner et al. 2004; Nabeshima et al. 2004).

A second CO pathway that is interference-independent has been uncovered in budding yeast, *Arabidopsis*, and mice, potentially complicating analysis of crossover interference in these organisms (Guillon et al. 2005; Whitby 2005). For example, the yeast mutation *zip1* was originally thought to disrupt interference (Sym and Roeder 1994), but it actually eliminates the interference-dependent COs and reveals interference-insensitive COs that are resolved through the Mus81/Mms4 pathway (de los Santos et al. 2003).

In comparison, *C. elegans* exhibits very tight control of meiotic crossing over: Only one CO occurs per chromosome pair per meiosis (Barnes et al. 1995; Meneely et al. 2002; Hillers and Villeneuve 2003), and COs appear to occur only through an interference-dependent pathway. This is not simply an average of one CO, since cytological analysis of oocyte meiosis shows that achiasmate chromosomes are extremely rare (Dernburg et al. 1998). This robust CO control makes *C. elegans* a particularly useful model to study the underlying mechanism.

We show that the number and distribution of COs are controlled by DPY-28. Reduction of DPY-28 activity increases the number of RAD-51 foci (suggestive of increased DSBs), elevates crossing over, biases the distribution of COs to recombination hot spots, and disrupts interference. Reduction of DPY-28 activity also partially restores DSBs in animals lacking HIM-17, a chromatin-associated protein required for DSB formation. These results suggest that DPY-28 functions early during meiotic recombination to limit DSBs. We propose that DPY-28, a DCC component that resembles a condensin subunit, mediates two different chromosome behaviors—regulation of gene expression, and control of CO number and distribution—through changes in chromosome structure.

Results

Cloning of dpy-28

dpy-28 was identified in a screen for mutations that disrupted dosage compensation and caused hermaphrodite-specific lethality (Plenefisch et al. 1989). The phenotypes caused by new mutations found in our noncomplementation (*y283* and *y284*) and deletion library (*y402*) screens resemble those in the original mutants: XX-specific lethality, dumpiness, and an increase in X-chromosome nondisjunction (Supplemental Material).

To dissect the role of *dpy-28* in dosage compensation, we cloned the gene using a combination of approaches (Fig. 1A,B). *dpy-28* was positioned on the physical map in the interval between cosmids W04F9 and M142 using genetic markers and then mapped more precisely to the gap between cosmids K01G5 and K11D9 using restriction fragment length polymorphisms (RFLPs) (Fig. 1A; Supplemental Material). RNAs corresponding to 34

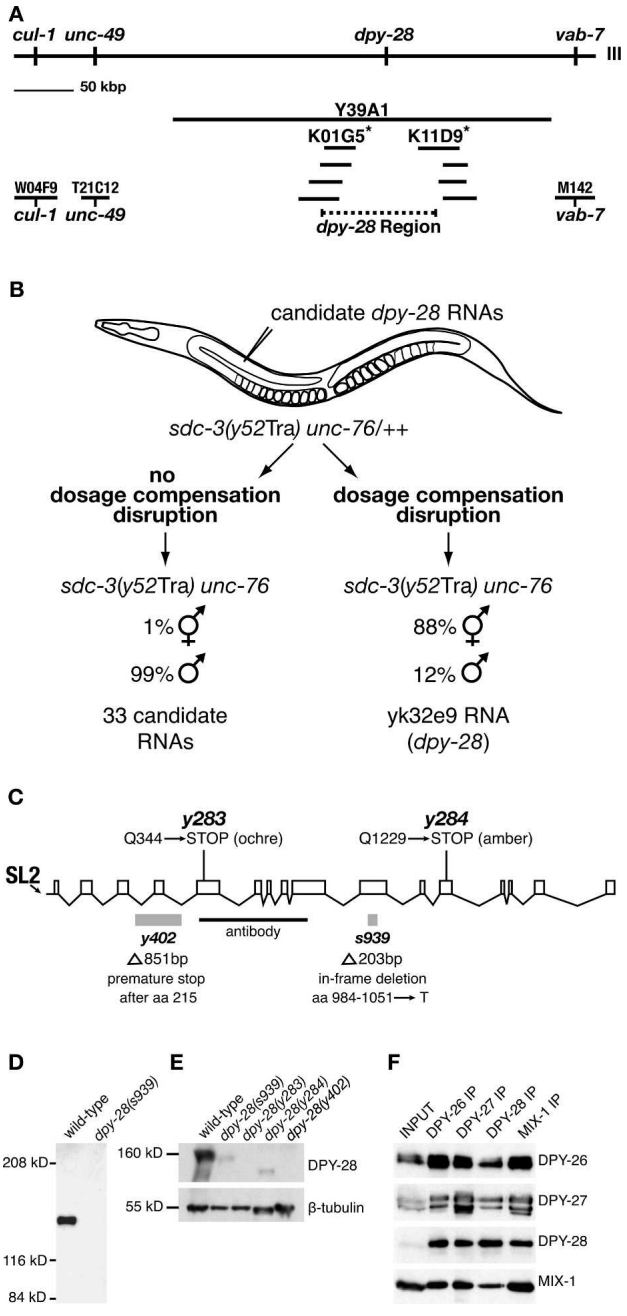

Figure 1. Molecular analysis of *dpy-28*. (*A*) Corresponding genetic and physical maps of chromosome III near *dpy-28*. *dpy-28* was mapped to the interval between markers *cul-1* (on W04F9) and *vab-7* (on M142) and then between RFLPs (asterisks) on cosmids K01G5 and K11D9. (*B*) RNAi assay identifying *dpy-28*. Candidate *dpy-28* RNAs were injected into *sdc-3(*Tra*) unc-76/++* XX animals, and F1 Unc progeny were scored for hermaphrodites. F1 Unc homozygous *sdc-3(*Tra*) unc-76* XX progeny from untreated heterozygous mothers develop as pseudomales. This transformed (Tra) phenotype is reversed by *dpy-28* mutations (DeLong et al. 1993). RNA corresponding only to cDNA yk32e9 suppressed the Tra phenotype and caused all phenotypes typical of *dpy-28* mutants. (*C*) *dpy-28* gene structure. Promoter, exons, and introns are represented by a horizontal line, boxes, and diagonal lines, respectively. Molecular changes in four *dpy-28* alleles are shown. DPY-28 antibodies were made against amino acids 351–771 (black bar). (*D*) Western blot of extracts from wild-type and *dpy-28(s939)* embryos probed with DPY-28 antibodies. DPY-28 migrates at ~160 kDa and is undetectable in *s939* embryonic extract. (*E*) Western blot of lysates from wild-type and *dpy-28* gravid adult hermaphrodites probed with antibodies to DPY-28 and β-tubulin, the loading control. Changes in DPY-28 level and size are consistent with molecular lesions in the mutants. (*F*) DPY-28 coimmunoprecipitates with known members of the DCC. Reciprocal coimmunoprecipitation of DPY-26, DPY-27, DPY-28, and MIX-1 with antibodies to each of the four proteins indicates that DPY-28 is a subunit of the DCC.

families of cDNAs expressed from the *dpy-28* region were assessed for their ability to phenocopy *dpy-28* mutations in an RNAi assay (Fig. 1B; Supplemental Material). Only RNA to cDNA yk32e9 caused the phenotypes characteristic of *dpy-28* mutants.

The *dpy-28* gene has 15 introns, spans 14,226 base pairs (bp) from the SL-2 *trans*-spliced leader site to the polyadenylation site, and encodes a predicted protein of 1499 amino acids (166 kDa) (Fig. 1C). The *s939* allele has an in-frame deletion that replaces codons 984–1051 with a threonine codon. *y402* has an 851-bp deletion that causes premature translation termination after amino acid 215. Codons 344 and 1229 of *y283* and *y284*, respectively, are nonsense codons. A second gene resides 192 bp upstream of the *dpy-28 trans*-splice site, implying that *dpy-28* is a downstream gene in an operon, consistent with the SL-2 leader on its mRNA.

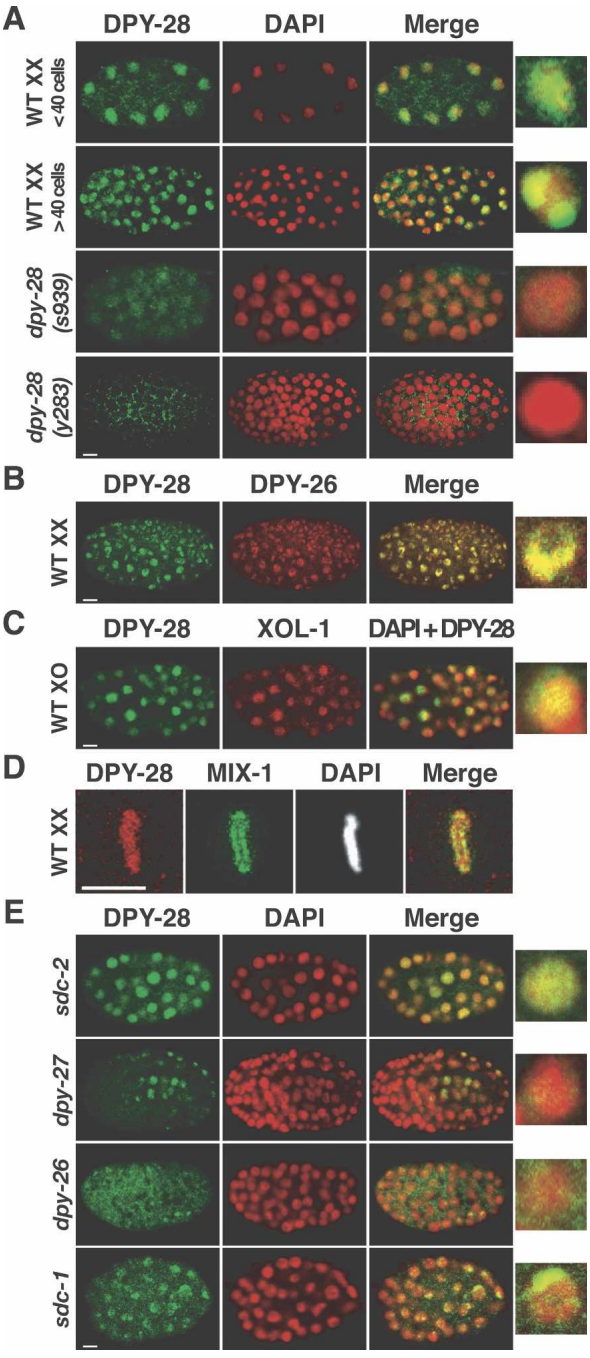

Figure 2. DPY-28 associates with X chromosomes of XX but not XO embryos. (*A*) Immunolocalization of DPY-28 in XX embryos. Shown are false-color confocal images of wild-type and *dpy-28* mutant XX embryos costained with DPY-28 antibodies (green) and the DNA-intercalating dye DAPI (red). Overlap of DPY-28 and DAPI appears yellow in merged images. An enlarged, merged nucleus is shown for each genotype. The diffuse nuclear DPY-28 pattern in young embryos and the punctate DPY-28 pattern in older embryos with ≥40 cells are absent in *dpy-28(s939)* or *dpy-28(y283)* mutants. (*B*,*C*) DPY-28 associates with X chromosomes of XX but not XO embryos. (*B*) DPY-28 colocalizes with X-bound DPY-26 in wild-type XX embryos. (*C*) A *him-8; yIs34(Pxol-1::gfp)* XO embryo with >40 cells costained with antibodies against DPY-28 (green) and XOL-1 (red). XOL-1::GFP is expressed exclusively in XO embryos, where DPY-28 appears diffuse nuclear. (*D*) DPY-28 (red) associates with mitotic chromosomes of young embryos prior to the onset of dosage compensation. DPY-28 colocalizes with DAPI on mitotic chromosomes, in contrast to mitotic condensin subunit MIX-1 (green), which colocalizes with centromeres (Hagstrom et al. 2002). (*E*) Association of DPY-28 with X requires other dosage compensation proteins. Shown are embryos with null mutations in various dosage compensation genes costained with DPY-28 antibodies (green) and DAPI (red). Bars, 5 µm.

DPY-28 is similar to the condensin component XCAP-D2

BLASTP searches of GenBank with the *dpy-28* sequence identified a protein family conserved from yeast to humans. The founding member, *Xenopus* 13S condensin subunit XCAP-D2, and related condensin proteins CND1 (*Schizosaccharomyces pombe*), YCS4 (*Saccharomyces cerevisiae*), HCP-6 (*C. elegans*), and CNAP1 (humans) promote mitotic chromosome compaction and segregation (Kimura et al. 1998; Sutani et al. 1999; Schmiesing et al. 2000; Bhalla et al. 2002; Chan et al. 2004). The similarity of DPY-28 to XCAP-D2 strengthens the connection between the DCC and condensin and increases the likelihood that the complexes utilize related mechanisms for diverse outcomes, fine-tuning X-linked gene expression during dosage compensation and achieving higher-order chromosome structure during mitosis.

Non-SMC proteins have both regulatory and structural roles in condensin. Their mitosis-specific phosphorylation is essential for condensin's ATP-stimulated activity in chromosome condensation (Kimura and Hirano 2000). Binding of non-SMC subunits to the SMC heterodimer restrains the accessibility of the SMC head domain to the DNA, resulting in dispersed binding along the DNA via the hinge region (Yoshimura et al. 2002). DPY-28 is required for the stability of SMC subunits in the DCC and for their binding to X, consistent with its

similarity to XCAP-D2 (Chuang et al. 1996; Lieb et al. 1998).

DPY-28 is a component of the DCC

We showed that DPY-28 forms a complex with other DCC subunits in vivo by raising DPY-28 antibodies and performing immunoprecipitation experiments. A protein of ~160 kDa was identified by Western analysis of wild-type but not *dpy-28(s939)* embryonic extracts (Fig. 1D) or *dpy-28(y283)* and *dpy-28(y402)* adult worm extracts (Fig. 1E). Truncated proteins of reduced abundance were found in *dpy-28(s939)* and *dpy-28(y284)* extracts (Fig. 1E). These results are consistent with the molecular lesions in the mutants. The ~160-kDa protein corresponds in size to a component of the biochemically defined DCC (Chuang et al. 1996).

DPY-28 antibodies immunoprecipitated DPY-28 and DCC subunits DPY-26, DPY-27, and MIX-1 from wild-type but not *dpy-28(s939)* embryonic extracts (Fig. 1F; data not shown). In reciprocal experiments, antibodies to DPY-26, DPY-27, and MIX-1 immunoprecipitated DPY-28 and the other DCC proteins, establishing DPY-28 as a DCC member (Fig. 1F).

DPY-28 associates with mitotic chromosomes prior to the onset of dosage compensation and with hermaphrodite X chromosomes after the onset

A DCC component should localize to X chromosomes of XX but not XO embryos by the 40-cell stage, when dosage compensation is activated. We observed a punctate, subnuclear DPY-28 staining pattern in wild-type XX embryos with ≥40 cells (Fig. 2A) that was absent in *dpy-28(s939)* and *dpy-28(y283)* mutants (Fig. 2A). The punctate pattern coincided with the X-chromosome staining of DPY-26 antibodies, indicating that DPY-28 localizes to hermaphrodite X chromosomes (Fig. 2B). Hermaphrodite-specific X localization of DPY-28 was shown using a transgenic reporter expressed exclusively in males (Fig. 2C). XO embryos exhibit diffuse nuclear DPY-28 staining instead of punctate staining characteristic of X localization (Fig. 2C). These results confirm DPY-28 as a bona fide component of the DCC.

In young, wild-type XX embryos prior to the onset of dosage compensation, DPY-28 is distributed diffusely in interphase nuclei, as in XO embryos, and becomes associated with all condensed chromosomes during mitosis, exhibiting complete overlap with DAPI (Fig. 2A,D). The mitotic chromosome staining is absent in *dpy-28(y283)* embryos (Supplemental Fig. 1). This mitotic pattern (Fig. 2D) is similar to that of DPY-26 (Lieb et al. 1996), yet it differs from that of the mitotic condensin protein MIX-1 (Hagstrom et al. 2002), which colocalizes with centromere proteins at the poleward face of condensed mitotic chromosomes. The difference in DPY-28 and MIX-1 patterns suggests that the proteins act independently.

DPY-28 is mislocalized or greatly reduced in dosage compensation mutants

DPY-26, DPY-27, and MIX-1 depend on each other and dosage compensation proteins SDC-2, SDC-3, and DPY-30 for their X localization (Chuang et al. 1996; Lieb et al. 1996, 1998). We examined DPY-28 localization in dosage compensation mutants to determine whether it has similar requirements. DPY-28 failed to assemble onto X chromosomes in *sdc-2*, *sdc-3*, and *dpy-30* mutants but instead had a diffuse nuclear distribution, like other DCC subunits (Fig. 2E; data not shown). Mutations in *dpy-26* or *dpy-27* greatly reduced DPY-28 levels and abolished DPY-28 X localization (Fig. 2E), consistent with DPY-26, DPY-27, and DPY-28 forming a complex that requires all subunits for stability. Like DPY-26 and DPY-27, DPY-28 appeared punctate in *sdc-1* and *dpy-21* mutant embryos (Fig. 2E; data not shown), showing that SDC-1 and DPY-21 are dispensable for binding of the DCC to X. In summary, DPY-28 behaves like other DCC subunits in its requirements for X localization and stability.

DPY-28 accumulates throughout the germline

While examining DPY-28 localization, we found that DPY-28 accumulates throughout the germline, a tissue that lacks the DCC. A series of immunostaining experiments revealed the germline distribution of DPY-28. Germline nuclei in both hermaphrodite gonad arms are arranged in an ordered, temporal progression that includes premeiotic stages, meiotic stages, and embryos (see Fig. 3A for diagram). In the premeiotic region, DPY-28 has a speckled nuclear pattern that partly overlaps with DNA in interphase nuclei (Fig. 3B), but is excluded from condensed mitotic chromosomes (data not shown). DPY-28 is more concentrated on chromosomes in the transition zone, when homologs began to pair, and appears unevenly distributed (Fig. 3B). In pachytene nuclei, DPY-28 is in the nucleoplasm and partly coincident with meiotic chromosomes, but is excluded from the nucleolus (Fig. 3B). No staining was detected above background in *s939*, *y283*, or *y402* gonads (Fig. 3C; data not shown), consistent with our Western analysis. The distribution of DPY-28 in male gonads is similar (data not shown).

dpy-28 mutations cause chromosome segregation defects in germline mitosis

Consistent with DPY-28 accumulation in the premeiotic germline, mitotic chromosome segregation defects occur in *dpy-28* mutant germlines. In *s939*, *y283*, or *y402* mutant gonads, some premeiotic nuclei were unusually large and had clumps of DNA (macronuclei) (Fig. 3D), while others were unusually small (micronuclei). Fluorescence in situ hybridization (FISH) analysis to assess ploidy using a 5S rDNA probe showed that the majority of *s939* premeiotic germ nuclei had two signals, indicating correct ploidy. However, a subset of germ nuclei had

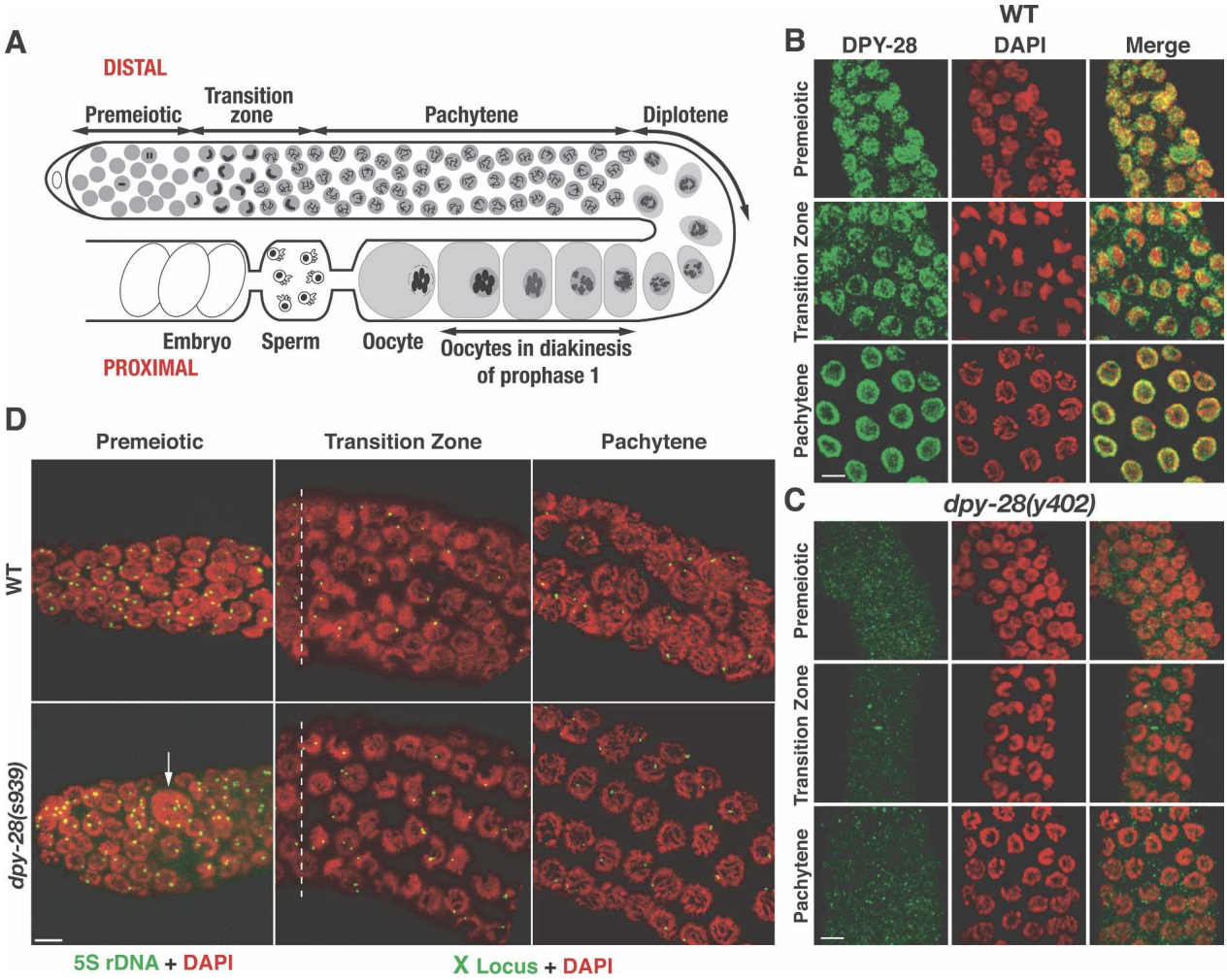

Figure 3. DPY-28 accumulates in germline nuclei, and *dpy-28* mutants are defective in mitotic chromosome segregation but progress normally through meiotic prophase. (*A*) Diagram of adult hermaphrodite gonad arm. Each arm is a U-shaped tube that produces male and female gametes. Germ nuclei proliferate in the distal premeiotic zone, then enter meiosis and progress through meiotic prophase stages as they move proximally. In the transition zone, homologs pair and initiate synapsis. Synapsis is complete prior to pachytene, and recombination ends during pachytene. Disassembly of the SC and condensation of homologs by condensin II begin at pachytene exit. At diakinesis, each oocyte nucleus has six DAPI-stained bodies that correspond to six pairs of recombined homologs. (*B*,*C*) DPY-28 accumulates in wild-type but not *dpy-28(y402)* mutant germlines. Shown are regions of hermaphrodite gonads stained with DAPI (red) and DPY-28 antibodies (green). In wild-type gonads, DPY-28 accumulates in premeiotic nuclei and remains nuclear in the meiotic transition zone, partially coincident with DAPI. In pachytene, DPY-28 concentrates around the nuclear periphery, where meiotic chromosomes reside. (*D*) FISH analysis of gonads stained with DAPI (red) and FISH probes 5S rDNA or X locus (green). Premeiotic nuclei of wild-type and *dpy-28(s939)* gonads typically have two FISH signals, indicating normal ploidy, but *dpy-28* mutants have occasional macronuclei (arrow) with multiple FISH signals, indicating aneuploidy or polyploidy. Wild-type and *dpy-28* mutant nuclei have two FISH signals in early transition zone before homolog synapsis and one signal in mid- to late transition zone and in pachytene, indicating normal homolog synapsis. Premeiotic and transition zones (shown in full length) are of equivalent length in wild-type and *dpy-28* mutants. The dashed white lines separate a single row of premeiotic nuclei from transition zone nuclei. Bars, 5 µm.

greater or fewer than two FISH signals (Fig. 3D), indicating missegregation of mitotic chromosomes.

dpy-28 mutations increase meiotic CO recombination and disrupt crossover interference on X chromosomes and autosomes

We assessed the role of DPY-28 in meiosis by assaying a hallmark event, CO recombination (Fig. 4). The effects of *dpy-28* mutations on crossing over were examined by analyzing the segregation of snip-SNP markers, single nucleotide polymorphisms (SNPs) that are RFLPs (Supplemental Table 1). Scoring multiple snip-SNP markers along individual chromatids allowed us to assess three aspects of crossing over: CO frequency in any given interval, distribution of COs, and the number of COs on a single chromatid.

A 40-cM interval corresponding to 80% of the X chro-

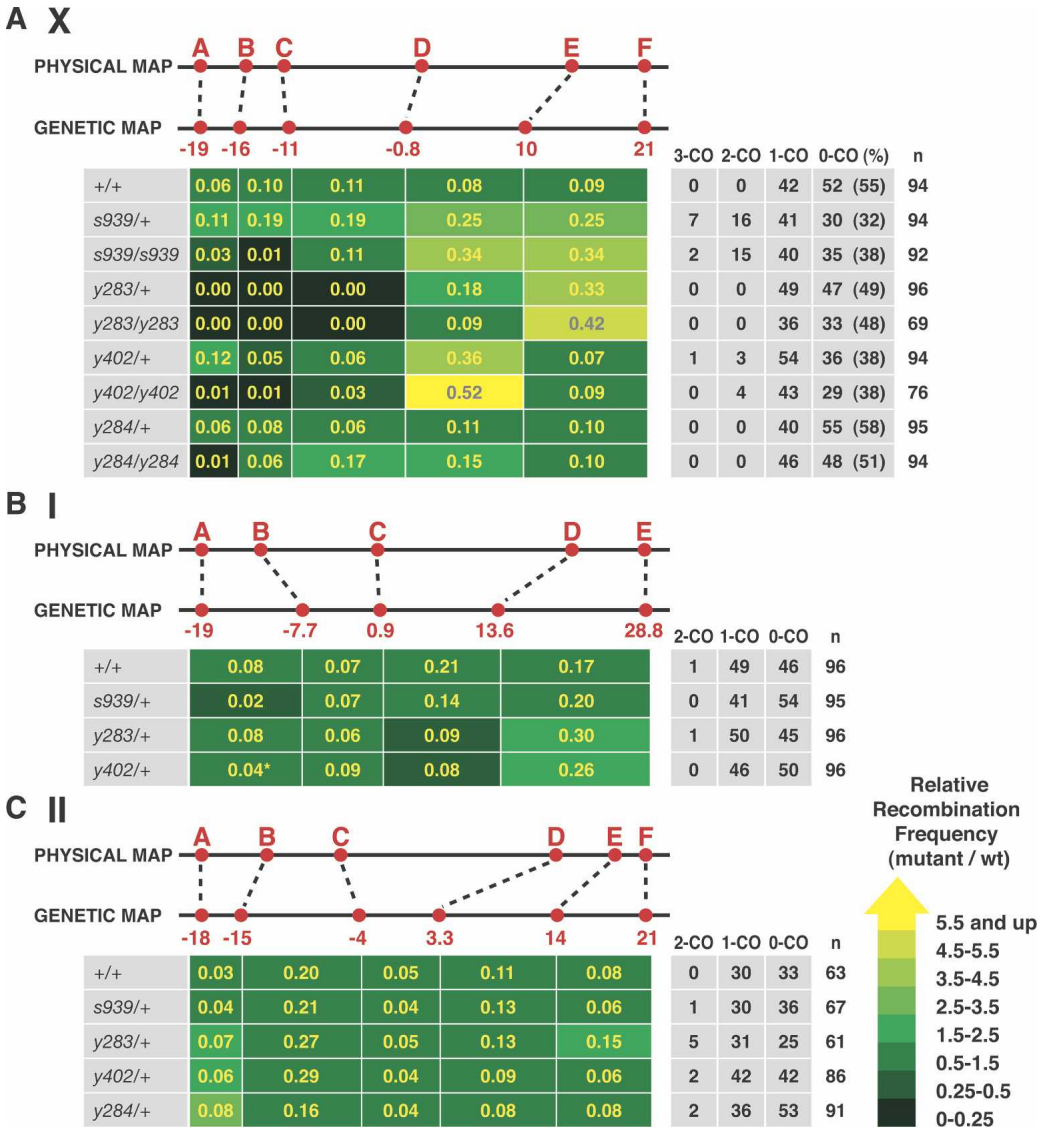

Figure 4. *dpy-28* mutations alter the number and distribution of COs on X chromosomes and autosomes. (*A–C*) CO analysis of chromosomes X, I, and II in wild-type and *dpy-28* mutant animals using snip-SNPs. Physical and genetic map positions of the snip-SNP markers (red) are shown *above* the CO frequency chart. CO frequencies (yellow numbers in boxes) were calculated by assessing recombination in the intervals between snip-SNPs and applying the formula (number of COs in the interval)/(total meiotic products assayed). Shown are the number of triple-crossover (3-CO), double-crossover (2-CO), single-crossover (1-CO), and noncrossover (0-CO) chromatids and total assayed chromatids (n). (%) Percentage of 0-COs by the formula 100(0-CO/n). The relative recombination frequencies (mutant/wild type) are indicated by color tags. Yellow reflects the greatest increase and black reflects the greatest decrease. (*A*) Heterozygous and homozygous *dpy-28* mutations *s939*, *y283*, or *y402* affect meiotic crossing over on X. Five intervals between snip-SNP markers A–F were assayed for recombination. For all *dpy-28* mutant alleles, CO frequencies were elevated in the right half and depressed in the left half. Also, 2-COs and 3-COs occurred in heterozygous and homozygous *s939* and *y402* animals. Map expansion and contraction is diagrammed in Supplemental Figure 2. (*B*) *s939*/+, *y283*/+, and *y402*/+ exert a milder effect on crossing over on chromosome I versus X. Four intervals between snip-SNP markers A–E were assayed. (*) For analysis of *y402*/+ animals, marker B* (genetic position, –12.3) was used instead of B. The wild-type CO frequency of the A–B* interval is 0.04 and the B*–C interval is 0.03. The relative CO frequency in *y402*/+ animals is compared with these values. (*C*) *s939*/+, *y283*/+, *y402*/+, and *y284*/+ cause 2-COs on chromosome II. Five intervals between snip-SNP markers A–F were assayed. See the Supplemental Material for details.

mosome was assayed using six snip-SNPs (A–F) (Fig. 4A). Control animals had the normal number and distribution of COs (total recombination frequency, 0.45) and showed the expected complete interference: No more than one CO was detected on any single chromatid. In contrast, homozygous and heterozygous *s939*, *y283*, or *y402* animals exhibited an increase in CO number and/or an overall redistribution of COs (Fig. 4A; diagrammed in Supplemental Fig. 2). The extent of increase was interval-dependent and ranged from no significant changes

to increases several times the wild-type frequency on the right half of X, between markers D and F ($P < 10^{-5}$ for *s939*, *y283*, or *y402*). Significant reduction of CO frequency was noted in the left half of X, between markers A and D, in homozygous *y283* and *y402* mutants ($P < 10^{-5}$) and *y283*/+ mutants ($P < 10^{-7}$). In fact, no crossing over occurred within this interval in *y283* mutants, and all the COs were shifted to the right half of X, greatly expanding the genetic distance between markers D and F. The dominant nature of *dpy-28* mutations on crossing over is likely due to haploinsufficiency, since both *y283* and *y402* mutations introduce early stop codons, and no protein products were detected in either mutant (Figs. 1E, 2A). CO recombination on X in *y284*/+ animals appeared similar to that of control animals, but in *y284*/*y284* animals CO frequency was decreased in the A–B interval and increased in the C–D and D–E intervals. Thus, *y284* appears to act like a hypomorph in both dosage compensation and recombination. In summary, reduction of *dpy-28* activity increased COs on X and biased CO distribution to the right half of X.

In addition to increasing CO frequency and altering CO distribution, *s939* and *y402* mutations also reduced crossover interference on X in a dominant fashion. Double-crossover (2-CO) and triple-crossover (3-CO) products were readily detected in heterozygous and homozygous *s939* and *y402* animals (Fig. 4A; Supplemental Table 2). For example, 16 2-COs and seven 3-COs were found in 94 chromatids assayed from *s939*/+ animals. The corresponding 2-CO or 3-CO ratios, [(2-CO or 3-CO)/(1-CO + 2-CO + 3-CO)], were 0.25 and 0.11, respectively, while both ratios were 0 for the control (Supplemental Table 2). Moreover, 10 of 16 2-COs and five of seven 3-COs involved COs that occurred in adjacent intervals, D–E and E–F (Supplemental Table 3).

Besides 2-CO and 3-CO ratios, coefficients of coincidence (CoC) (see Supplemental Table 2 for calculations) were used to assess crossover interference. A CoC of 0, as calculated from control animals, indicates complete interference; no 2-COs or 3-COs were detected in the intervals examined. A CoC of 1 indicates that COs occur independently of one another; i.e., no interference is displayed between the intervals. A CoC of >1 indicates negative interference; a CO in one interval increases the likelihood of a CO in the other interval. CoCs for the X chromosome as a whole are 1.0 for *s939*/*s939* or *y402*/*y402* animals, 0.72 for *y402*/+ animals, and 1.0 for *s939*/+ animals, showing that *dpy-28* mutations greatly reduce or eliminate crossover interference (Supplemental Table 2). CoCs were also calculated using only intervals D–E and E–F, which have the highest 2-CO frequencies on X (Supplemental Table 2). For the *s939*/*s939* example, the value is 1.4, showing that many 2-COs are confined to the right side of X, and the disruption of crossover interference is uneven along X.

We noted that non-CO (0-CO) chromatids were underrepresented in *dpy-28* mutants. In control animals, 0-CO chromatids represented 55% of total X chromatids assayed (Fig. 4A). However, in *s939*/+, *s939*, *y402*/+, and *y402* animals, 0-CO products represented 32%, 38%, 38%, and 38% of the respective X chromatids assayed ($P < 0.01$) (Fig. 4A). This phenomenon may be explained in two ways. First, reduction of *dpy-28* function allows more than two chromatids to participate in the reciprocal exchange between a pair of homologs, resulting in the reduction of 0-CO products. Second, 0-CO products are preferentially lost during meiotic chromosome segregation. We favor the first explanation, in part because no meiotic X nondisjunction events were observed in heterozygous *dpy-28* animals, but we cannot rule out the second possibility.

The effect of *dpy-28* mutations on meiotic recombination is general (Fig. 4B,C; Supplemental Tables 4, 5). For chromosome I, both *y283*/+ and *y402*/+ mutations caused a redistribution of COs (Fig. 4B; Supplemental Fig. 2). Crossing over was increased in the interval between markers D and E ($P < 0.03$), and decreased in the adjacent interval between markers C and D ($P < 0.03$). However, the overall recombination frequency between markers A and E (0.49) did not change, and no increase in 2-CO or 3-CO products was found in *s939*/+, *y283*/+, and *y402*/+ animals. On chromosome II, the number of COs was slightly elevated in the left half (interval A–C) and remained unchanged in the center of the chromosome (interval C–D) in *y283*/+ and *y402*/+ animals (Fig. 4C). 2-CO products were detected in heterozygous *s939*/+, *y283*/+, *y402*/+, and *y284*/+ animals. The chromosome-wide CoCs ranged from 0.2 to 0.5, showing reduction of crossover interference (Supplemental Tables 4, 5). For the specific intervals with the highest 2-COs, the CoCs ranged from 0.5 to 2, showing elimination of interference for those intervals (Supplemental Tables 4, 5).

dpy-28 mutations affected crossing over to different degrees on the three chromosomes, but changes in CO distribution were found on all three chromosomes. Disruption of crossover interference was pronounced for chromosomes X and II, but an increase in CO frequency was evident only for X. Because *dpy-28*/+ animals produced wild-type numbers of viable progeny and exhibited no X-chromosome nondisjunction, we reasoned that every homolog pair in *dpy-28*/+ animals must have at least one CO, and the total number of COs for each nucleus likely exceeds the obligatory six found in wild-type worms.

CO formation in dpy-28(s939) animals requires SPO-11 and MSH-5

To assess whether the increase in COs in *dpy-28* mutants was due to overactivation of the normal pathway or instead to a novel pathway, we analyzed combinations of *dpy-28* mutations and mutations that block CO formation. In *C. elegans*, SPO-11-generated DSBs are the initiating lesions for most, if not all, meiotic recombination, and the meiosis-specific MutS ortholog MSH-5 is required to resolve recombination intermediates into COs (Dernburg et al. 1998; Colaiacovo et al. 2003). In *spo-11* or *msh-5* single mutants, no COs occur between

homologs; thus, 12 DAPI-stained bodies (univalents) are observed routinely at diakinesis. In 20 *dpy-28(s939); spo-11(ok79)* double mutants examined, only diakinesis nuclei with 12 DAPI-stained bodies were found, indicating no COs. Similarly, 12 DAPI-stained bodies were observed in 129/129 diakinesis nuclei of *dpy-28(s939); msh-5(me23)* double mutants. These results suggest that CO initiation and resolution occur in *dpy-28* mutants via the same pathway as in wild-type animals.

Meiotic progression and SC formation appeared normal in dpy-28 mutants

Hillers and Villeneuve (2003) proposed that crossover interference in *C. elegans* is conferred by the continuity of chromosome axes. If *dpy-28* mutations reduce interference by disrupting assembly of contiguous chromosome axes, we would expect to find discontinuity in the localization of axis- or SC-associated proteins. Furthermore, homolog pairing and synapsis would be impaired in *dpy-28* mutants if their axes were defective (Zetka et al. 1999). We first examined the effects of *dpy-28* mutations on chromosome morphology and homolog pairing in meiotic prophase with fluorescence microscopy. In wild-type or *dpy-28* gonads stained with DAPI, no obvious cytological difference was seen prior to diakinesis. The premeiotic, transition, and pachytene regions spanned similar distances, and *dpy-28* mutants exhibited no delayed entry into any given stage (Fig. 3D). Furthermore, no difference was observed in homolog pairing between wild-type and *dpy-28* animals as judged by FISH (Fig. 3D). Nuclei in both premeiotic regions and both early transition zones had two FISH signals, indicating homologs had not yet paired, as expected. In both mid- to late transition zones, FISH signals were close or paired. Homologs remained paired throughout pachytene. These results show that homolog pairing and synapsis are not perturbed in *dpy-28* mutants.

Axis and SC assembly were examined in *s939* and *y283* mutants by immunofluorescence using antibodies to HIM-3, an axis-associated protein (Zetka et al. 1999), and SYP-1, a component of the SC central region (MacQueen et al. 2002). Immunolocalization of both HIM-3 and SYP-1 appeared indistinguishable in *dpy-28* and wild-type animals (Fig. 5A), indicating that *dpy-28* mutations do not cause gross disruption of the axis or SC. To exclude the possibility that the SC was disrupted at the ultrastructural level in *dpy-28* mutants and hence was not detectable by immunostaining, we used transmission electron microscopy (TEM). A typical tripartite SC structure was found in both wild-type and *dpy-28(s939)* pachytene nuclei, including a pronounced ladder-like central element, similar to previous ultrastructural analysis of the *C. elegans* SC (Fig. 5B,C; Dernburg et al. 1998). Moreover, contiguous stretches of SC were observed as frequently in sections from *dpy-28* mutants as from wild-type animals. We conclude that the continuity of the axis and SC is not disrupted in *dpy-28* mutants.

RAD-51-bound recombination intermediates are increased in dpy-28 mutants

In budding yeast, high levels of local DSBs are correlated with regions of elevated recombination and vice versa (Wu and Lichten 1994; Petes 2001). Since *dpy-28* mutations increase COs, we asked whether extra COs correlated with induction of more DSBs. To address this issue, we identified nascent recombination intermediates, and thereby estimated the number of DSBs formed during meiosis, using antibodies against *C. elegans* RAD-51, the ortholog of *S. cerevisiae* Rad51 involved in strand invasion/exchange during homologous recombination (Colaiacovo et al. 2003).

In wild-type gonads, RAD-51 foci are rare in the premeiotic region, first appear consistently in the transition zone, peak in early to mid-pachytene, and disappear by pachytene exit (Fig. 6A; Supplemental Fig. 3; Colaiacovo et al. 2003). In *dpy-28(s939)* and *dpy-28(y283)* mutant gonads, the progression of RAD-51 foci resembles that of wild-type gonads, but more RAD-51 foci occur per nucleus in early to mid-pachytene of *dpy-28* mutants (Fig. 6A–C; Supplemental Fig. 3; data not shown). RAD-51 focus formation in *dpy-28* mutants is DSB-dependent, since it requires SPO-11 (Fig. 6B,C).

Quantification of RAD-51 foci assessed the increase in foci caused by *dpy-28* mutations (Fig. 6A). In early pachytene (P1), the wild-type to *dpy-28(s939)* comparison was 84% versus 40% of nuclei with two to six foci, and 23% versus 52% of nuclei with seven to 12 foci. In mid-pachytene (P2), the wild-type to mutant comparison was 76% versus 58% of nuclei with two to six foci, and 3% versus 23% of nuclei with seven to 12 foci. In late pachytene (P3), the wild-type to mutant comparison was 10% versus 5% of nuclei with two to six foci and 1% versus 2% of nuclei with seven to 12 foci. Thus, *dpy-28* mutations increase RAD-51 foci, and likely meiotic DSBs, without perturbing the normal progression of meiotic recombination.

The increase in RAD-51-bound recombination intermediates in dpy-28 mutants reflects an increase in DSB production

The increased steady-state level of RAD-51 foci in *dpy-28* mutants could reflect either a true increase in DSB production or a delay in DSB repair. To discriminate between these two possibilities, we blocked the completion of COs in wild-type animals and *dpy-28* mutants by disrupting the recombination protein MSH-5 or the SC structural protein SYP-2 and then compared the profile of RAD-51 foci throughout meiotic prophase. Animals depleted of MSH-5 or SYP-2 produce wild-type levels of RAD-51 foci, but the foci are not resolved in a timely manner (Colaiacovo et al. 2003). Rather, the foci persist into late pachytene. If *dpy-28* mutations caused only delayed resolution of early recombination intermediates, we would expect to find a similar accumulation of unresolved RAD-51 foci in pachytene of *dpy-28; msh-5* or *dpy-28; syp-2* double mutants as in *msh-5* or *syp-2* single

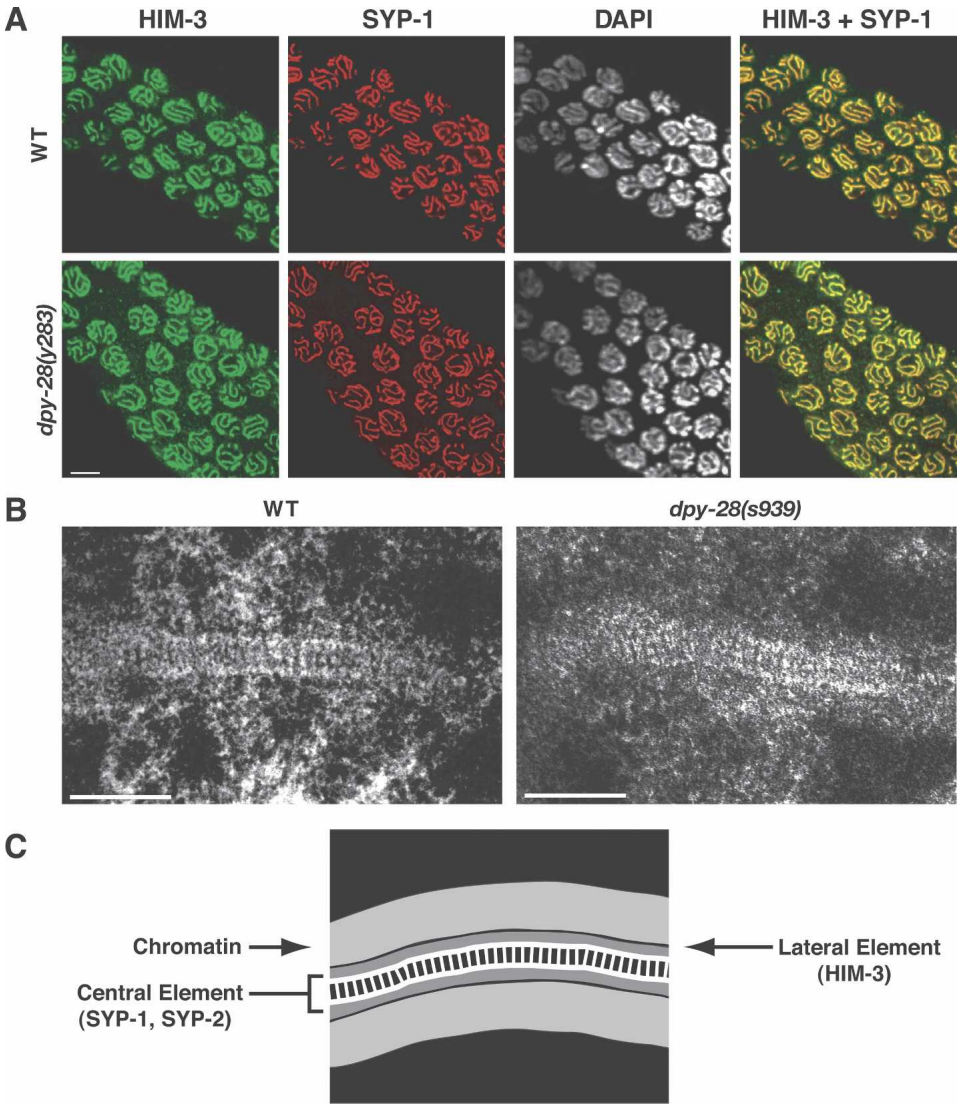

Figure 5. The axes and SC appear wild type in *dpy-28* mutants. (*A*) In false-color confocal images of *dpy-28(y283)* pachytene nuclei, the axis component HIM-3 (green) and the SC component SYP-1 (red) colocalize (yellow merge) along the entirety of homologs, as in wild-type controls. Bar, 5 µm. (*B*) Sections of SC in pachytene nuclei of wild-type and *dpy-28(s939)* gonads visualized by transmission electron microscopy. In both genotypes, the SC appears continuous, and the transverse filaments between lateral elements appear as rung-like structures. Bars, 200 nm. (*C*) A schematic of the SC structural components and chromatin.

mutants. In fact, more RAD-51 foci were observed in the double mutants ($P = 7 \times 10^{-5}$ for *dpy-28; msh-5* and 0.002 for *dpy-28; syp-2*) (Fig. 7A,B; Supplemental Fig. 4). In both double mutants, the increase in RAD-51 foci mirrored that in *dpy-28* mutants, and the foci persisted into late pachytene as in *msh-5* or *syp-2* single mutants. These results indicate that the increase in RAD-51 foci in *dpy-28* mutants most plausibly represents an increase in DSB formation and not persistence of early recombination intermediates involving RAD-51.

Increased RAD-51 foci in dpy-28(s939) animals require the axis component HIM-3

The worm axis-associated protein HIM-3 is required for homolog pairing and synapsis (Zetka et al. 1999). In addition, HIM-3 helps bias meiotic CO recombination between homologs rather than sister chromatids. Without HIM-3, homologs cannot pair or synapse; nevertheless, normal levels of RAD-51 foci appear and disappear with wild-type kinetics (Couteau et al. 2004), suggesting that DSB initiation is unaffected in *him-3* mutants, but DSB repair is carried out using sister chromatids as templates. Although HIM-3 is not essential for DSB formation in wild-type animals, we postulated that the increased RAD-51 foci in *dpy-28* mutants might still be HIM-3- or axis-dependent, since axes are crucial for organizing meiotic chromosomes, and elevated DSB formation might reflect altered chromosome structure. We assessed the number and distribution of RAD-51 foci in *dpy-28(s939); him-3(gk149)* double mutants and found them to be

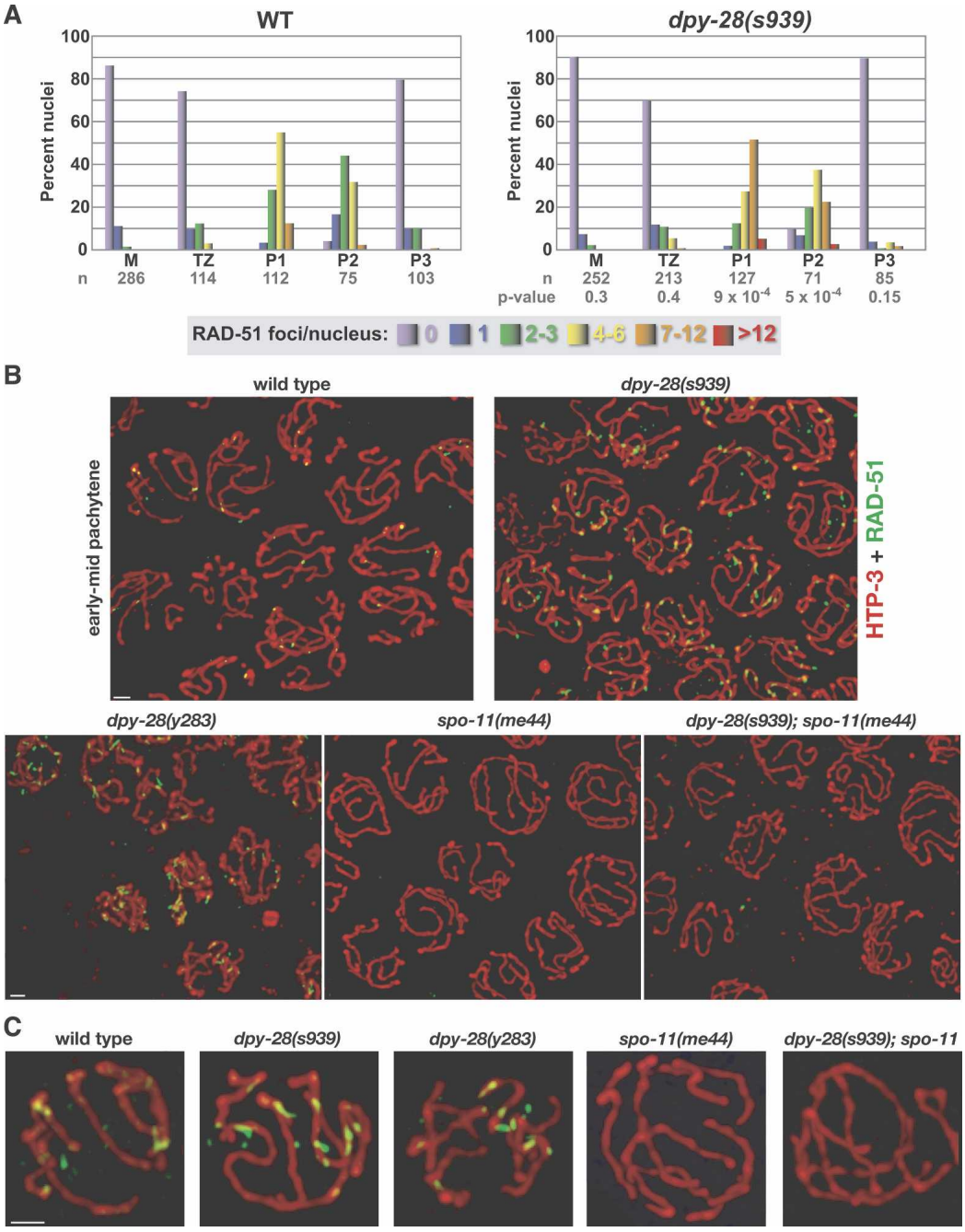

Figure 6. *dpy-28* mutants show an increase in DSB-dependent early recombination intermediates but normal progression of these RAD-51 foci. (*A*) Histograms depicting quantitation of RAD-51 foci in wild-type and *dpy-28(s939)* germlines. Each column color represents a class of nuclei with the indicated number of RAD-51 foci. The *Y*-axis shows the percentage of nuclei in each class. The *X*-axis shows the position along the germline. (M) Premeiotic zone; (TZ) transition zone; (P1) early pachytene; (P2) mid-pachytene; (P3) late pachytene; (n) number of nuclei scored. *P*-values from χ^2 tests show that the distribution of RAD-51 foci is different in wild-type and mutant germlines, with a significant increase in P1 and P2 of *s939*. (See the Supplemental Material for details). (*B*,*C*) The increase in RAD-51 foci in *dpy-28* mutants requires the DSB enzyme SPO-11. Shown are high-resolution images of wild-type and mutant early to mid-pachytene nuclei stained with antibodies to RAD-51 (green) and the axis protein HTP-3 (red). (*C*) Enlarged nuclei from *B*. Bars, 1 μm.

similar to those in *him-3* single mutants (*P*-values for pachytene regions are 0.3, 0.05, and 0.09) (Fig. 7C; Supplemental Fig. 4). These results indicate that HIM-3 is required for DPY-28's role in regulating DSB formation in meiosis.

dpy-28(s939) suppresses CO defects in him-17(null) animals

DSB formation in *C. elegans* requires HIM-17, a chromatin-associated protein (Reddy and Villeneuve 2004). *him-*

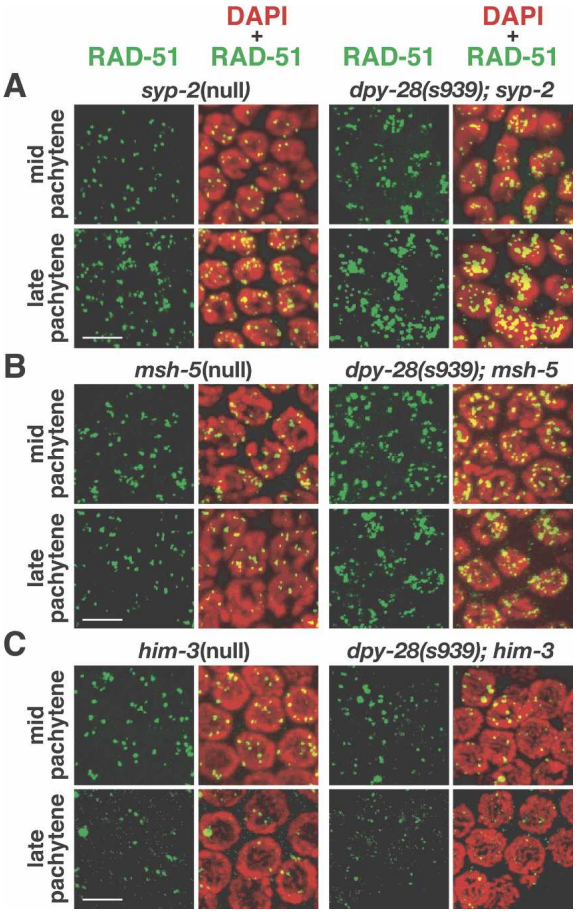

Figure 7. *dpy-28* mutants require MSH-5 and SYP-2 for the resolution of RAD-51-bound recombination intermediates and HIM-3 for the increase in RAD-51 foci. All panels are false-color confocal images of germline nuclei stained with DAPI (red) and RAD-51 antibodies (green). (*A*,*B*) SC core component SYP-2 and mismatch repair protein MSH-5 are required for the timely removal of RAD-51 foci in wild-type and *dpy-28* animals. In *syp-2* and *msh-5* single mutants and in *dpy-28; syp-2* and *dpy-28; msh-5* double mutants, RAD-51 foci persist into late pachytene, indicating impaired resolution of meiotic recombination intermediates (Fig. 6). In double mutants, the number of RAD-51 foci is elevated, as in *dpy-28* mutants, suggesting that more meiotic DSBs are made in *dpy-28* mutants, and their repair requires SYP-2 and MSH-5. (*C*) Axis component HIM-3 is required in *dpy-28* mutants for the increase in RAD-51 foci. *dpy-28; him-3* double mutants have a similar number of RAD-51 foci as *him-3* mutants. Without HIM-3, *dpy-28* mutations do not cause an increase in meiotic DSBs. Quantification for *A–C* is in Supplemental Figure 4. Bars, 5 µm.

17(*ok424*-null) animals lack RAD-51 foci and chiasmata, yet exhibit normal homolog pairing and synapsis. γ-Irradiation restores chiasma formation in *him-17* mutants, showing that the recombination machinery for converting DSBs into COs is intact. *him-17* interacts genetically with the worm Rb homolog *lin-35.* Mammalian Rb proteins associate with chromatin-remodeling enzymes, such as the histone deacetylase HDAC1, to alter chromatin structure and thereby control gene expression (for review, see Macaluso et al. 2006). HIM-17 also affects histone methylation in pachytene, but apparently after DSB formation. Reddy and Villeneuve (2004) proposed that HIM-17 promotes DSB formation through effects on chromatin structure. We postulated that DPY-28, a CAP-D2 homolog, might have the opposite effect. DPY-28 could restrict DSBs by influencing higher-order chromosome structure, since CAP-D2 homologs act in condensin to modulate overall chromosome organization during mitosis and meiosis (Chan et al. 2004; for review, see Losada and Hirano 2005). To test this hypothesis, we explored genetic interactions between *dpy-28* and *him-17*.

To assess chiasmata, we scored the number of DAPI-stained bodies in diakinesis nuclei of *dpy-28(s939); him-17(ok424)* double mutants (Fig. 8A,B). Wild-type and *dpy-28* animals had six DAPI-stained bodies in 97% and 90%, respectively, of diakinesis nuclei, showing that at least one chiasma usually formed in each of the six homolog pairs. In contrast, 43% of diakinesis nuclei in *him-17* mutants contained 12 DAPI-stained bodies, consistent with the lack of chiasmata reported by Reddy and Villeneuve (2004). Supporting our hypothesis, *dpy-28(s939)* partially suppressed the *him-17(ok424)* CO defect. Chiasmata were greatly elevated in double mutants compared with *him-17* single mutants, as indicated by the reduction of DAPI-stained bodies per diakinesis nucleus. Of 45 diakinesis nuclei from double mutants, 0% had 12 DAPI-stained bodies, 60% had seven bodies, and 18% had six bodies (Fig. 8B).

To assess DSB formation, we examined RAD-51 foci in *him-17* single and *dpy-28; him-17* double mutants (Fig. 8C). As expected, we found more RAD-51 foci in double mutants than in single mutants, consistent with the increase in chiasmata noted above. In early pachytene (P1) (Fig. 8C), the following comparison of RAD-51 foci was found between *dpy-28; him-17* double mutants and *him-17* single mutants: 73% versus 94% of nuclei with zero foci, 17% versus 6% of nuclei with one to three foci, and 8% versus 0% of nuclei with four to 12 foci. In mid-pachytene (P2) (Fig. 8C), the comparison of RAD-51 foci between *dpy-28; him-17* double mutants and *him-17* single mutants was 64% versus 92% of nuclei with zero foci, 25% versus 8% of nuclei with one to three foci, and 11% versus 0% of nuclei with four to 12 foci. These data demonstrate that *dpy-28(s939)* partially suppresses the DSB initiation and CO defects in *him-17* mutants, and suggest that DPY-28 controls meiotic recombination prior to or at the time of DSB formation. Furthermore, this global effect may be mediated through changes in higher-order chromosome structure.

Discussion

We demonstrated that an essential component of the *C. elegans* DCC regulates CO number and distribution during meiosis. Dosage compensation and CO regulation require chromosome-wide communication to achieve distinct goals, the coordinated repression of genes dispersed along a whole chromosome, and the regulation of

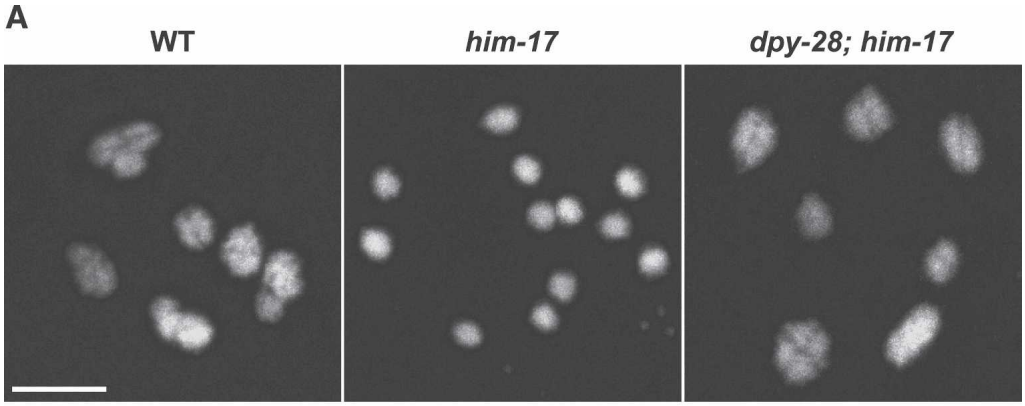

B

Genotype	Percent oocyte nuclei with the indicated number of DAPI bodies								N
	5	6	7	8	9	10	11	12	
wild-type	3	97	0	0	0	0	0	0	31
dpy-28(s939)	2	90	8	0	0	0	0	0	97
him-17(ok424)	0	0	0	2	12	23	20	43	60
him-17(ok424)[a]	0	0	0	2	5	14	14	65	58
dpy-28(s939); him-17(ok424)	0	18	60	11	9	2	0	0	45

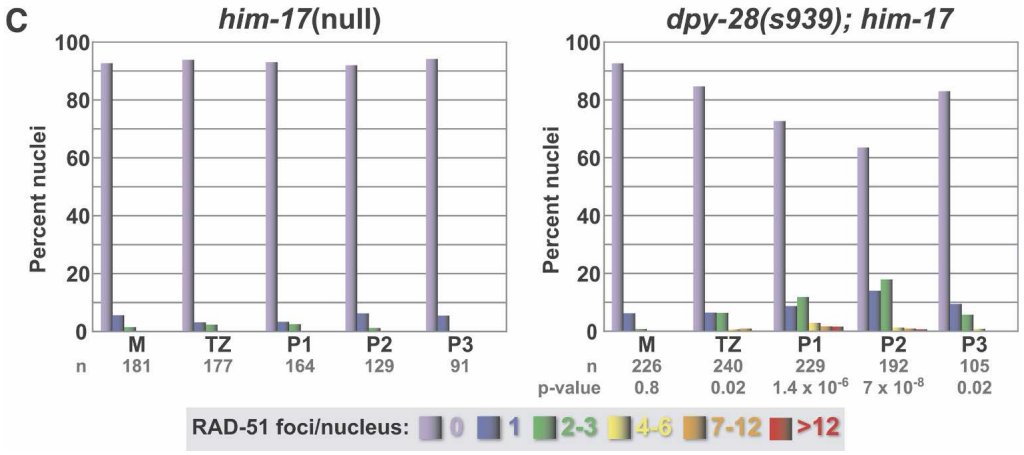

Figure 8. The CO and DSB defects of *him-17*(null) mutants are suppressed by *dpy-28(s939)*. (*A*) DAPI-stained oocyte nuclei in late diakinesis from wild-type, *him-17(ok424)*, or *dpy-28(s939); him-17(ok424)* animals. Each panel shows a set of chromosomes from one oocyte. The wild-type oocyte has six bivalents, indicating normal chiasma formation. Most *him-17* oocytes have 12 univalents, reflecting a lack of chiasmata. Most *dpy-28; him-17* oocytes have seven DAPI-stained bodies, including five bivalents and two univalents. Bar, 5 µm. (*B*) Karyotype analysis of diakinesis-stage oocytes. *him-17(ok424)*[a] denotes the *him-17(ok424)* strain reisolated from the *dpy-28; him-17* strain. (*C*) Quantitation of RAD-51 foci in *him-17* and *dpy-28; him-17* germlines shows increased foci in double mutants. *P*-values from χ^2 tests indicate that the distribution of RAD-51 foci is different in wild-type and mutant germlines. Each column color represents a class of nuclei with the indicated number of RAD-51 foci. The *Y*-axis shows the percentage of nuclei in each class and the *X*-axis shows the position along the germline. (M) Premeiotic zone; (TZ) transition zone; (P1) early pachytene; (P2) mid-pachytene; (P3) late pachytene.

crossing over to ensure one CO per homolog pair while discouraging COs nearby. The protein linking these two global processes has extensive similarity with *Xenopus* XCAP-D2, a condensin non-SMC subunit that acts with SMC proteins to facilitate chromosome compaction, resolution, and segregation. The discovery of DPY-28 strengthens the parallel between the DCC and condensin and reveals a previously unknown role for condensin components in limiting the exchange of DNA between homologs. Both processes likely utilize related mechanisms involving the restructuring of chromosomes to attain chromosome-wide effects.

DPY-28 promotes germline mitosis independently of defined C. elegans *condensin complexes*

DPY-28 also functions in chromosome segregation during germline mitosis, as revealed by FISH analysis in *dpy-28* mutants. While it is not surprising for an XCAP-D2 homolog to engage in chromosome segregation in the context of a condensin complex, it is unlikely that DPY-28's function in germline mitosis occurs through participation in either known *C. elegans* condensin complex, condensin II or the DCC. First, biochemical analysis of *C. elegans* condensin II identified a different CAP-D2 homolog, HCP-6, as a partner for the SMC components MIX-1 and SMC-4 (Chan et al. 2004). Second, unlike condensin II components, which localize to condensed chromosomes, DPY-28 appears excluded from germline mitotic chromosomes. Third, the segregation phenotypes caused by *dpy-28*-null mutations are not as severe or as penetrant as those caused by disruption of genes encoding condensin II subunits (Hagstrom et al. 2002). Consistent with these arguments, DPY-28 and MIX-1 differ in localization on mitotic chromosomes of early embryos. MIX-1 staining colocalizes with centromeres, while DPY-28 staining resembles DAPI. Finally, it is improbable that DPY-28 carries out its germline function in the context of the DCC because the DCC component DPY-27, a paralog of SMC-4, fails to exhibit premeiotic germline accumulation and, when depleted, fails to cause missegregation of germline mitotic chromosomes.

Control of CO number and distribution by DPY-28

C. elegans is an attractive organism for analyzing CO control because it displays complete interference: Once a CO site is designated, crossover interference suppresses all other COs on the same chromosome (Hillers and Villeneuve 2003). We show that DPY-28 participates in the regulation of CO number and distribution. Specifically, reduction of *dpy-28* activity increased the number of RAD-51 foci and concomitantly increased crossing over along X chromosomes and autosomes by permitting 2-COs and 3-COs, unlike in wild-type animals. Moreover, most 2-COs on X occurred within 20 cM on the right side, exhibiting clear disruption of crossover interference. The COs required SPO-11 and MSH-5, suggesting that meiotic recombination in *dpy-28* mutants is mediated through the canonical pathway, rather than an alternative pathway. Thus, one role of DPY-28 is to restrict COs, likely by disfavoring formation of DSBs.

The number of 0-COs is lower in *dpy-28* mutants than in wild-type animals, but the reduction is not sufficient to account for the CO increase in *dpy-28* mutants. That is, the recombination frequency in mutants is higher than the sum of the 1-CO frequency in wild-type animals plus the difference in 0-CO frequency between wild-type and *dpy-28* animals. Moreover, *dpy-28; msh-5* double mutants have more RAD-51 foci than *msh-5* single mutants. Thus, decrease of *dpy-28* activity does not simply convert 0-CO-destined DSBs to COs.

As in many organisms, COs in *C. elegans* occur more frequently on the terminal thirds of each chromosome rather than on the middle third. A plot of genetic intervals (*Y*-axis) against physical distance (*X*-axis) defined by cloned genes revealed that specific regions of a chromosome show elevated CO activity, referred to as hot spots (Supplemental Fig. 5A–C). Of interest, two of the prominent hot spots, those located in the right ends of chromosomes I and X, were made hotter by *dpy-28* mutations, which permit even more COs to occur.

Different mechanisms can underlie an increase in COs

The mechanism by which *dpy-28* mutations perturb CO number and distribution appears distinct from those of previously characterized *C. elegans* mutations, which resulted in different patterns of COs. In mutants that failed X chromosome synapsis because of a recessive *him-8* mutation, Carlton et al. (2006) observed a delay in the reorganization of all chromosomes during early meiotic prophase and a concomitant perdurance of RAD-51 foci. That delay perturbed the normal pattern of COs on autosomes. For example, on chromosomes III and V, CO number increased in the middle of the chromosomes, which are normally CO-deficient, causing a more even distribution of COs along the entire chromosome length rather than a bias toward the ends. In contrast, *dpy-28* mutations altered CO distribution in the opposite order, increasing COs on the chromosome ends and away from the center. Moreover, *dpy-28* mutations did not cause an apparent delay in the progression of meiotic prophase: Meiotic chromosome pairing and synapsis appeared indistinguishable from the wild-type control by FISH analysis. Correspondingly, the appearance and disappearance of RAD-51 foci in *dpy-28* animals followed wild-type kinetics. Thus, the extra COs in *dpy-28* and *him-8* mutants appear to have different causes.

Nabeshima et al. (2004) showed that defective axis assembly also alters the pattern of COs. *him-3* encodes a component of the *C. elegans* chromosome axis that is homologous to the *S. cerevisiae* axis protein Hop1p (Zetka et al. 1999). The missense, partial loss-of-function mutation *him-3(me80)* caused discontiguous axis and SC assembly and reduced the overall number of COs per meiosis. Nevertheless, the fragmented axis and SC were able to support some crossing over, resulting in a subset of homolog pairs with more than one CO amidst the majority of homologs that failed to have any. In *him-3(me80)* mutants, homolog pairing and synapsis were disrupted and showed delayed kinetics. Coincidentally, RAD-51 foci persisted into mid- to late pachytene. In light of the CO pattern in the X synapsis mutant characterized by Carlton et al. (2006), perturbation of CO control by *him-3(me80)* may be attributable, at least in part, to delayed resolution of RAD-51-bound recombination intermediates. The axis defects caused by *him-3(me80)* do not pertain to the change in CO pattern achieved by *dpy-28* mutations, because axis and SC assembly, as assessed by immunofluorescence and TEM analyses, showed no evidence of structural discontinuity in *dpy-28* mutants. We propose instead that DPY-28 restricts meiotic crossing over through its effects on the

establishment or maintenance of meiotic chromosome structure.

A link between chromosome structure, DSBs, and crossover interference by DPY-28

Chromatin context is known to influence DSB location. In budding yeast, DSBs reside in open chromatin (Wu and Lichten 1994), as assessed by increased micrococcal nuclease sensitivity, which occurs just prior to DSB formation (Ohta et al. 1994). However, open local chromatin is not sufficient for DSB formation. For example, a recombination reporter exhibits low DSB levels when inserted into CO cold spots and high DSB levels when inserted into hot spots, despite both locations having the same pattern and levels of DNase I hypersensitivity (Wu and Lichten 1995; Borde et al. 1999). Thus, higher-order chromosome structure, such as differential chromatin compaction or region-specific localization within the nucleus, has been proposed to contribute to the differences in DSB frequencies between chromosomal regions.

Multiple lines of evidence suggest that DPY-28 links chromosome structure to DSB formation and to the control of CO number and distribution. First, the resemblance of DPY-28 to the XCAP-D2 subunit of condensin, a complex required for chromosome resolution and compaction, suggests that DPY-28 participates in organizing chromosome structure. Indeed, the DPY-28 paralog HCP-6 loads onto meiotic chromosomes at pachytene exit and is essential for the reorganization of chromosomes into their compact structures during diplotene and diakinesis (Chan et al. 2004). Second, the increase in RAD-51 foci, a marker for DSBs, and the redistribution of COs are both haploinsufficient phenotypes. The strict dose-dependence of DPY-28 function is consistent with the role of a structural protein limited in supply to achieve proper chromosome organization. Third, *dpy-28* mutations suppress the loss of DSB formation caused by mutations in *him-17*, which encodes a chromatin-associated protein required for germline histone modification. In the absence of HIM-17, very few DSBs are created. Inactivation of DPY-28 partially restores DSBs and COs in *him-17*-null animals, suggesting that *dpy-28* mutations compensate for the change in chromatin architecture. As germ cells progress from premeiotic S phase into meiosis, DPY-28 could act in opposition to HIM-17 by controlling a higher-order level of chromosome structure and thereby modulate DSB formation. Fourth, the increase in RAD-51 foci in *dpy-28* mutants requires the axis protein HIM-3, suggesting a functional link between DPY-28 and chromosome axes and/or axis-associated proteins in organizing chromosome architecture.

Chromosome organization is a key component in a model for crossover interference by Kleckner et al. (2004). They proposed that meiotic chromosomes are under mechanical stress. This stress promotes CO formation, which in turn releases stress around the CO site for a certain distance along the chromosome and discourages crossing over nearby. In their model, the mechanical stress can be generated by organizational and functional interactions between chromatin, chromosomal structural proteins, chromosome axes, and the axis-associated proteins. In support of the model, the DNA base composition in the budding yeast genome (GC-rich segments and AT-rich segments) affects localization of axis-associated proteins such as Red1p, which in turn affects the distribution of COs (Blat et al. 2002). Specifically, Red1p binds preferentially to the axes in GC-rich segments and facilitates loading of the meiosis-specific RecA homolog Dmc1p to DSBs in these regions. Consistent with Dmc1p localization, meiotic recombination hot spots reside mostly in the GC-rich regions of chromosome arms and away from the central AT-rich region.

The *C. elegans* genome differs from the genomes of budding yeast and humans in that its GC content is essentially constant (36%) across all chromosomes (The *C. elegans* Genome Consortium 1998; Wilson 1999). Nevertheless, the CO distribution along a *C. elegans* chromosome is similar to that along a budding yeast or human chromosome—more COs occur in the terminal one-third of the chromosome and fewer in the middle third. We surmise that the mechanisms governing DSB formation and CO control are likely to be conserved, at least in part, between budding yeast and worms, despite the lack of discernible partitioning of GC-rich and AT-rich regions in the worm genome. In *C. elegans*, chromosomal structural proteins may play a more prominent role in organizing meiotic chromosomes to compensate for the lack of GC-rich regions.

A potential difference exists between the mechanisms that underlie CO regulation in yeast versus worms. Yeast chromosomes have a surplus of DSBs compared with COs (on average, 60 ± 18 Rad51p/Dmc1p foci to ~30 COs per nucleus) (Shinohara et al. 2000), and DSBs can be matured into COs via two pathways, interference-dependent and interference-independent. In contrast, worm chromosomes exhibit complete interference and have a lower ratio of DSBs to COs (on average approximately five plus or minus two RAD-51 foci to six COs per nucleus), implying that DSB number limits, at least in part, the number of COs. We propose that the number and placement of DSBs are constrained in worms by higher-order chromosome structure achieved in part by DPY-28, and DSB placement contributes to CO distribution. In this model, *dpy-28* mutants would have a chromosome structure more permissive for DSB initiation in specific domains of meiotic chromosomes and hence an increase in RAD-51-bound recombination intermediates. Potentially, the more permissive structure could also exert a greater expansional force and increase mechanical stress to influence DSB resolution, contributing to the biased redistribution of COs to distinct chromosomal regions and disruption of interference.

Context of DPY-28 function

Although DPY-28's function in meiotic recombination is unlikely to be dependent on the two defined *C. elegans*

condensin complexes, the DCC and condensin II, DPY-28 may partner with SMC or SMC-like proteins to carry out its activity. Protein complexes containing SMC subunits participate in diverse chromosome functions throughout the cell cycle (for review, see Hagstrom and Meyer 2003). Such complexes have the capacity to exert global effects on chromosome architecture and thereby promote chromosome-wide communication, a strategy that may well underlie how a protein with strong resemblance to a condensin subunit regulates CO number and distribution in one context and X-chromosome gene repression in another.

Materials and methods

CO analysis

For CO analysis, Bristol N2 and CB4856 *C. elegans* isolates were used because their chromosomes have a sequence polymorphism every 1.5–2 kb. To assess COs on X, *dpy-28/dpy-28* or *dpy-28*/+ hermaphrodites with heterozygous N2/CB4856 X chromosomes were made by first crossing *dpy-28* males with CB4856 hermaphrodites, mating male-cross progeny that carried CB4856 X with *unc-32 dpy-28/qC1[qIs26]* hermaphrodites. F1 non-Unc non-Rol hermaphrodites were picked to individual plates for a 24-h embryo collection, then crossed with N2 males, and their male cross-progeny were scored for SNP markers using single worm PCRs and restriction digestions with appropriate endonucleases. F1 hermaphrodites that produced dead self-progeny were *dpy-28/dpy-28*. F1s that produced all viable self-progeny were *dpy-28*/+. For control crosses, *unc-32*/+ males were mated with CB4856 hermaphrodites, and the hermaphrodite cross-progeny of genotype *unc-32*/+ were identified by the presence of Unc self-progeny in the F2 generation. Six SNP markers were chosen along the X chromosome based on their map positions (Supplemental Table 1).

To assess COs on chromosomes I and II, *dpy-28/qC1[qIs26]* hermaphrodites were mated with CB4856 males. F1 non-Rol hermaphrodites were first picked to individual plates to lay embryos for 24 h to eliminate homozygous *dpy-28* self-progeny and then crossed with wild-type N2 males. The F2 male cross-progeny were scored for SNP markers as above. SNP markers are listed in Supplemental Table 1.

Immunostaining

Embryo immunostaining was as in Dawes et al. (1999). Germline immunofluorescence and FISH staining were as in Chan et al. (2004). A detailed protocol is in the Supplemental Material.

Topics included in the Supplemental Material

The following information is provided in the Supplemental Material: strains used in the study, screens for *dpy-28* mutations, genetic mapping of *dpy-28*, RFLP analysis of *dpy-28*, cDNA identification for RNAi assays to define *dpy-28*, sequence identification of *dpy-28* mutations, list of primers used, antibody preparation, immunoprecipitation and immunoblot analysis, immunostaining, DAPI analysis, and time-course analysis for RAD-51 foci.

Acknowledgments

We thank A. Severson and I. Carmi for critical comments on the manuscript; T. Cline, E. Ralston, and A. Villeneuve for discussions; K. McDonald for help with TEM; A. Gartner for RAD-51 antibodies; A. Villeneuve for SYP-1 antibodies; M. Zetka for HIM-3 antibodies; A. Dernburg for HTP-3 antibodies; and J. Gunther for help with figures. D.M. was supported by NIH predoctoral training grant T32-GM07127, and C.T., M.A., and D.M. were supported by T32-GM007232. Research was supported by NIH grant R01-GM30702. B.J.M. is an Investigator of the Howard Hughes Medical Institute.

References

Allers, T. and Lichten, M. 2001. Intermediates of yeast meiotic recombination contain heteroduplex DNA. *Mol. Cell* **8:** 225–231.

Barnes, T.M., Kohara, Y., Coulson, A., and Hekimi, S. 1995. Meiotic recombination, noncoding DNA and genomic organization in *Caenorhabditis elegans*. *Genetics* **141:** 159–179.

Bergerat, A., de Massy, B., Gadelle, D., Varoutas, P.C., Nicolas, A., and Forterre, P. 1997. An atypical topoisomerase II from Archaea with implications for meiotic recombination. *Nature* **386:** 414–417.

Bhalla, N., Biggins, S., and Murray, A.W. 2002. Mutation of *YCS4*, a budding yeast condensin subunit, affects mitotic and nonmitotic chromosome behavior. *Mol. Biol. Cell* **13:** 632–645.

Blat, Y., Protacio, R.U., Hunter, N., and Kleckner, N. 2002. Physical and functional interactions among basic chromosome organizational features govern early steps of meiotic chiasma formation. *Cell* **111:** 791–802.

Borde, V., Wu, T.C., and Lichten, M. 1999. Use of a recombination reporter insert to define meiotic recombination domains on chromosome III of *Saccharomyces cerevisiae*. *Mol. Cell. Biol.* **19:** 4832–4842.

Borner, G.V., Kleckner, N., and Hunter, N. 2004. Crossover/noncrossover differentiation, synaptonemal complex formation, and regulatory surveillance at the leptotene/zygotene transition of meiosis. *Cell* **117:** 29–45.

Carlton, P.M., Farruggio, A.P., and Dernburg, A.F. 2006. A link between meiotic prophase progression and crossover control. *PLoS Genet.* **2:** e12. doi: 10.1371/journal.pgen.0020012.

The *C. elegans* Sequencing Consortium. 1998. Genome sequence of the nematode *C. elegans*: A platform for investigating biology. *Science* **282:** 2012–2018.

Chan, R.C., Severson, A.F., and Meyer, B.J. 2004. Condensin restructures chromosomes in preparation for meiotic divisions. *J. Cell Biol.* **167:** 613–625.

Chuang, P.T., Albertson, D.G., and Meyer, B.J. 1994. DPY-27: A chromosome condensation protein homolog that regulates *C. elegans* dosage compensation through association with the X chromosome. *Cell* **79:** 459–474.

Chuang, P.T., Lieb, J.D., and Meyer, B.J. 1996. Sex-specific assembly of a dosage compensation complex on the nematode X chromosome. *Science* **274:** 1736–1739.

Colaiacovo, M.P., MacQueen, A.J., Martinez-Perez, E., McDonald, K., Adamo, A., La Volpe, A., and Villeneuve, A.M. 2003. Synaptonemal complex assembly in *C. elegans* is dispensable for loading strand-exchange proteins but critical for proper completion of recombination. *Dev. Cell* **5:** 463–474.

Couteau, F., Nabeshima, K., Villeneuve, A., and Zetka, M. 2004. A component of *C. elegans* meiotic chromosome axes at the interface of homolog alignment, synapsis, nuclear reorganization, and recombination. *Curr. Biol.* **14:** 585–592.

Dawes, H.E., Berlin, D.S., Lapidus, D.M., Nusbaum, C., Davis, T.L., and Meyer, B.J. 1999. Dosage compensation proteins targeted to X chromosomes by a determinant of hermaphrodite fate. *Science* **284:** 1800–1804.

de los Santos, T., Hunter, N., Lee, C., Larkin, B., Loidl, J., and Hollingsworth, N.M. 2003. The Mus81/Mms4 endonuclease

acts independently of double-Holliday junction resolution to promote a distinct subset of crossovers during meiosis in budding yeast. *Genetics* **164:** 81–94.

DeLong, L., Plenefisch, J.D., Klein, R.D., and Meyer, B.J. 1993. Feedback control of sex determination by dosage compensation revealed through *Caenorhabditis elegans sdc-3* mutations. *Genetics* **133:** 875–896.

Dernburg, A.F., McDonald, K., Moulder, G., Barstead, R., Dresser, M., and Villeneuve, A.M. 1998. Meiotic recombination in *C. elegans* initiates by a conserved mechanism and is dispensable for homologous chromosome synapsis. *Cell* **94:** 387–398.

Fung, J.C., Rockmill, B., Odell, M., and Roeder, G.S. 2004. Imposition of crossover interference through the nonrandom distribution of synapsis initiation complexes. *Cell* **116:** 795–802.

Gerton, J.L., DeRisi, J., Shroff, R., Lichten, M., Brown, P.O., and Petes, T.D. 2000. Inaugural article: Global mapping of meiotic recombination hotspots and coldspots in the yeast *Saccharomyces cerevisiae*. *Proc. Natl. Acad. Sci.* **97:** 11383–11390.

Guillon, H., Baudat, F., Grey, C., Liskay, R.M., and de Massy, B. 2005. Crossover and noncrossover pathways in mouse meiosis. *Mol. Cell* **20:** 563–573.

Hagstrom, K.A. and Meyer, B.J. 2003. Condensin and cohesin: More than chromosome compactor and glue. *Nat. Rev. Genet.* **4:** 520–534.

Hagstrom, K.A., Holmes, V.F., Cozzarelli, N.R., and Meyer, B.J. 2002. *C. elegans* condensin promotes mitotic chromosome architecture, centromere organization, and sister chromatid segregation during mitosis and meiosis. *Genes & Dev.* **16:** 729–742.

Hillers, K.J. and Villeneuve, A.M. 2003. Chromosome-wide control of meiotic crossing over in *C. elegans*. *Curr. Biol.* **13:** 1641–1647.

Hong, E.L., Shinohara, A., and Bishop, D.K. 2001. *Saccharomyces cerevisiae* Dmc1 protein promotes renaturation of single-strand DNA (ssDNA) and assimilation of ssDNA into homologous super-coiled duplex DNA. *J. Biol. Chem.* **276:** 41906–41912.

Hunter, N. and Kleckner, N. 2001. The single-end invasion: An asymmetric intermediate at the double-strand break to double-Holliday junction transition of meiotic recombination. *Cell* **106:** 59–70.

Keeney, S., Giroux, C.N., and Kleckner, N. 1997. Meiosis-specific DNA double-strand breaks are catalyzed by Spo11, a member of a widely conserved protein family. *Cell* **88:** 375–384.

Kimura, K. and Hirano, T. 2000. Dual roles of the 11S regulatory subcomplex in condensin functions. *Proc. Natl. Acad. Sci.* **97:** 11972–11977.

Kimura, K., Hirano, M., Kobayashi, R., and Hirano, T. 1998. Phosphorylation and activation of 13S condensin by Cdc2 in vitro. *Science* **282:** 487–490.

Kirkpatrick, D.T., Wang, Y.H., Dominska, M., Griffith, J.D., and Petes, T.D. 1999. Control of meiotic recombination and gene expression in yeast by a simple repetitive DNA sequence that excludes nucleosomes. *Mol. Cell. Biol.* **19:** 7661–7671.

Kleckner, N., Zickler, D., Jones, G.H., Dekker, J., Padmore, R., Henle, J., and Hutchinson, J. 2004. A mechanical basis for chromosome function. *Proc. Natl. Acad. Sci.* **101:** 12592–12597.

Lieb, J.D., Capowski, E.E., Meneely, P., and Meyer, B.J. 1996. DPY-26, a link between dosage compensation and meiotic chromosome segregation in the nematode. *Science* **274:** 1732–1736.

Lieb, J.D., Albrecht, M.R., Chuang, P.T., and Meyer, B.J. 1998. MIX-1: An essential component of the *C. elegans* mitotic machinery executes X chromosome dosage compensation. *Cell* **92:** 265–277.

Losada, A. and Hirano, T. 2005. Dynamic molecular linkers of the genome: The first decade of SMC proteins. *Genes & Dev.* **19:** 1269–1287.

Macaluso, M., Montanari, M., and Giordano, A. 2006. Rb family proteins as modulators of gene expression and new aspects regarding the interaction with chromatin remodeling enzymes. *Oncogene* **25:** 5263–5267.

MacQueen, A.J., Colaiacovo, M.P., McDonald, K., and Villeneuve, A.M. 2002. Synapsis-dependent and -independent mechanisms stabilize homolog pairing during meiotic prophase in *C. elegans*. *Genes & Dev.* **16:** 2428–2442.

Meneely, P.M., Farago, A.F., and Kauffman, T.M. 2002. Crossover distribution and high interference for both the X chromosome and an autosome during oogenesis and spermatogenesis in *Caenorhabditis elegans*. *Genetics* **162:** 1169–1177.

Meyer, B.J. 2005. X-chromosome dosage compensation. In *WormBook* (ed. The *C. elegans* Research Community), doi: 10.1895/wormbook.1.8.1, http://www.wormbook.org.

Nabeshima, K., Villeneuve, A.M., and Hillers, K.J. 2004. Chromosome-wide regulation of meiotic crossover formation in *Caenorhabditis elegans* requires properly assembled chromosome axes. *Genetics* **168:** 1275–1292.

Ogawa, T., Yu, X., Shinohara, A., and Egelman, E.H. 1993. Similarity of the yeast RAD51 filament to the bacterial RecA filament. *Science* **259:** 1896–1899.

Ohta, K., Shibata, T., and Nicolas, A. 1994. Changes in chromatin structure at recombination initiation sites during yeast meiosis. *EMBO J.* **13:** 5754–5763.

Petes, T.D. 2001. Meiotic recombination hot spots and cold spots. *Nat. Rev. Genet.* **2:** 360–369.

Plenefisch, J.D., DeLong, L., and Meyer, B.J. 1989. Genes that implement the hermaphrodite mode of dosage compensation in *Caenorhabditis elegans*. *Genetics* **121:** 57–76.

Reddy, K.C. and Villeneuve, A.M. 2004. *C. elegans* HIM-17 links chromatin modification and competence for initiation of meiotic recombination. *Cell* **118:** 439–452.

Schmiesing, J.A., Gregson, H.C., Zhou, S., and Yokomori, K. 2000. A human condensin complex containing hCAP-C–hCAP-E and CNAP1, a homolog of *Xenopus* XCAP-D2, colocalizes with phosphorylated histone H3 during the early state of mitotic chromosome condensation. *Mol. Cell. Biol.* **18:** 6996–7006.

Shinohara, M., Gasior, S.L., Bishop, D.K., and Shinohara, A. 2000. Tid1/Rdh54 promotes colocalization of Rad51 and Dmc1 during meiotic recombination. *Proc. Natl. Acad. Sci.* **97:** 10814–10819.

Sun, H., Treco, D., Schultes, N.P., and Szostak, J.W. 1989. Double-strand breaks at an initiation site for meiotic gene conversion. *Nature* **338:** 87–90.

Sun, H., Treco, D., and Szostak, J.W. 1991. Extensive 3′-overhanging, single-stranded DNA associated with the meiosis-specific double-strand breaks at the *ARG4* recombination initiation site. *Cell* **64:** 1155–1161.

Sung, P. 1994. Catalysis of ATP-dependent homologous DNA pairing and strand exchange by yeast RAD51 protein. *Science* **265:** 1241–1243.

Sutani, T., Yuasa, T., Tomonaga, T., Dohmae, N., Takio, K., and Yanagida, M. 1999. Fission yeast condensin complex: Essential roles of non-SMC subunits for condensation and Cdc2 phosphorylation of Cut3/SMC4. *Genes & Dev.* **13:** 2271–2283.

Sym, M. and Roeder, G.S. 1994. Crossover interference is abol-

ished in the absence of a synaptonemal complex protein. *Cell* **79:** 283–292.
Szostak, J.W., Orr-Weaver, T.L., Rothstein, R.J., and Stahl, F.W. 1983. The double-strand-break repair model for recombination. *Cell* **33:** 25–35.
Villeneuve, A.M. and Hillers, K.J. 2001. Whence meiosis? *Cell* **106:** 647–650.
Whitby, M.C. 2005. Making crossovers during meiosis. *Biochem. Soc. Trans.* **33:** 1451–1455.
Wilson, R.K. 1999. How the worm was won. The *C. elegans* genome sequencing project. *Trends Genet.* **15:** 51–58.
Wu, T.C. and Lichten, M. 1994. Meiosis-induced double-strand break sites determined by yeast chromatin structure. *Science* **263:** 515–518.
Wu, T.C. and Lichten, M. 1995. Factors that affect the location and frequency of meiosis-induced double-strand breaks in *Saccharomyces cerevisiae*. *Genetics* **140:** 55–66.
Yoshimura, S.H., Hizume, K., Murakami, A., Sutani, T., Takeyasu, K., and Yanagida, M. 2002. Condensin architecture and interaction with DNA: Regulatory non-SMC subunits bind to the head of SMC heterodimer. *Curr. Biol.* **12:** 508–513.
Yu, H.G. and Koshland, D.E. 2003. Meiotic condensin is required for proper chromosome compaction, SC assembly, and resolution of recombination-dependent chromosome linkages. *J. Cell Biol.* **163:** 937–947.
Zetka, M.C., Kawasaki, I., Strome, S., and Muller, F. 1999. Synapsis and chiasma formation in *Caenorhabditis elegans* require HIM-3, a meiotic chromosome core component that functions in chromosome segregation. *Genes & Dev.* **13:** 2258–2270.
Zickler, D. and Kleckner, N. 1999. Meiotic chromosomes: Integrating structure and function. *Annu. Rev. Genet.* **33:** 603–754.